AEGC Australasian Exploration Geoscience Conference Brisbane 2023

Enhancements to deterministic AEM inversion through better geometry constraints and a bunch-by-bunch algorithm

Ross Brodie
Geoscience Australia
Symonston ACT
ross.brodie@ga.gov.au

Shane Mulè
CSIRO
Kensington, WA
shane.mule@csiro.au

SUMMARY

We have enhanced the existing program for the 1D deterministic inversion of airborne electromagnetic data called *GALEISBSTDEM*. The new source code will be publicly released in 2023. The updates include a number of improvements to the usability of the code including additional input and output options, null value handling, data culling, parameter bounds and a better build system. A more conservative line-search has been employed for determining the regularisation parameter at each iteration and for the parameter-change vector step-lengths. This has improved the robustness of the convergence of the algorithm and substantially reduced the number of narrow vertical striation artefacts in conductivity sections. The new release will also include the functionality to perform an inversion on the combined amplitude of the response in the XZ-plane rather than on the X- and Z-vector component data. This removes the dependence of the receiver bird pitch on the modelled response and allows the data to be fitted more easily, resulting in more laterally coherent conductivity sections with fewer artefacts.

We have also introduced the concept of a bunch-by-bunch inversion in which several soundings are inverted in a single minimization problem. The bunch, or window of soundings, is then moved along the flight line until the full data set is inverted. The approach allows along-line constraints to be placed upon the layer conductivities as well as any elements of the system geometry that are being inverted for. This is a feature that cannot be attained with conventional sounding-by-sounding approach. In addition to the usual constraints on the smoothness of the vertical conductivity profile, various types of along-line constraints may optionally be applied. These include conventional linear smoothness constraints, plus we also add similarity constraints and what we call a cable-length constraint that we can apply to the inversion of the transmitter-receiver separation for fixed-wing AEM systems. The inclusion of the along-line constraints are designed to make the inversion of the elements of AEM system geometry more stable and realistic as they are constrained to follow a smooth trajectory that is dictated by the dynamics of a high-drag towed receiver bird. We find that the bunch-by-bunch approach has so far not delivered the degree of improvements in the level of data fitting for the X- and Z-vector component inversions that we had originally hoped for. However we are encouraged by some reduction in the level of data misfit and a corresponding improvement in the along-line smoothness of the inverted geometry parameters.

Key words: Inversion, deterministic, airborne, electromagnetic, constrained.

INTRODUCTION

In 2015 Geoscience Australia released a suite of software for the 1D modelling and inversion of airborne electromagnetic (AEM) data into the public domain (Brodie and Richardson, 2015). The software package is known as *GA-AEM* and is made available via a repository on *GitHub*® (https://github.com/GeoscienceAustralia/ga-aem). The most used program in the *GA-AEM* package to date has been a deterministic regularised inversion that inverts each time-domain AEM sample/sounding independently (i.e., sample-by-sample) via a gradient-based down-hill search which is called ***GALEISBSTDEM***. The algorithm is based on the regularised inversion method described by (Constable *et al.*, 1987) and importantly includes the functionality to invert for system geometry parameters. The theoretical development of the *GALEISBSTDEM* algorithm is described by Brodie (2015).

Since the June 2016 release, when Matlab and Python interfaces were added to the forward modelling functionality, the GA-AEM package has only seen minor maintenance updates on the public-facing master branch of the repository. The *GALEISBSTDEM* code has been predominantly used in the inversion of data for Geoscience Australia's continental-scale AusAEM acquisition program (Ley-Cooper and Richardson, 2018) and internationally by the USGS for inversion of TEMPEST® data from the Mississippi Valley (Minsley *et al.*, 2021). The code has also been taken up by industry for inversion of their own surveys (Fitzpatrick and Whitford, 2019) and at least one AEM contractor (Combrinck *et al.*, 2022).

This abstract provides an update on new developments of the *GALEISBSTDEM* algorithm. These include the functionality to invert amplitude data that was completed in 2018, and more notably improvements made during a CSIRO funded collaboration with Geoscience Australia. This collaboration had a focus on improving the constraints

on system geometry parameter inversion, particularly to assist in the inversion of legacy AEM data which typically had no or poor measurement of system geometry. The main new functionality from this project are additional constraint types and the development of a method to invert a bunch of soundings to enable local lateral constraints on the along-line variation of system geometry. The paper will first provide detail on the previously completed amplitude inversion work, then outline several other usability improvements made during the collaboration project, before describing the new bunch-by-bunch inversion approach, which we expect to release in May 2023.

FUNCTIONALITY IMPROVEMENTS

XZ-Amplitude Inversion

The *GALEISBSTDEM* program now includes the optional functionality to invert the combined amplitude of the X- and Z-component data rather than the conventional approach of inverting the X- and Z-component data, either jointly, or separately. When this option is chosen, the input data d_w and assigned noise standard deviation σ_w for the wth window are respectively,

$$d_w = \sqrt{{x_w}^2 + {z_w}^2}, \;\; and \;\; \sigma_w = \sqrt{\frac{(x_w \sigma_w^x)^2 + (z_w \sigma_w^z)^2}{{x_w}^2 + {z_w}^2}}, \qquad (1)$$

where x_w, σ_w^x, z_w, σ_w^z refer to X- and Z-component data and assigned noise standard deviations for the wth window respectively. The rationale for this formulation is that there is then only a need to solve for the Tx-Rx horizontal and vertical separations. There is no need to invert for receiver-pitch because the XZ-amplitude data is not dependent (is insensitive to) receiver pitch. This approach was implemented for the AusAEM program and was reported by Ley-Cooper *et al.* (2019) in which improved along-line coherency and interpretability of conductivity-depth sections was demonstrated.

Usability

Several other minor but helpful new features of *GALEISBSTDEM* have been added to make the user workflow more flexible and efficient. These include: (a) Input/output of ASEGGDF2 format files including catering for some common errors in the definition files; (b) outputs to various header file formats including CSV; (c) handling of null and zero-valued data; (d) the functionality to variably cull individual windows from the inversion of each sample by use of the null data values; (e) functionality to set hard bounds on the inversion parameters; (f) additional error and warnings messages and more sanity checks on input parameters; (g) the ability to pass ancillary data fields, not used in the inversion, through to the output file; (h) experimental implementation of input/output using Geoscience Australia's NetCDF line-data format. Additionally, the *CMAKE* build system is now supported in an attempt to ease the burden of compiling and installing the source code on either Linux or Windows.

We have also implemented the optional functionality to delay the start of inversion for geometry parameters until after a set number of iterations to avoid unrealistically large geometry changes in the early iterations. A further improvement has been to make the line-search for both the regularisation parameter and the parameter change step-length more conservative. While requiring more forward models per sample, this has improved the robustness of the inversion.

Similarity constraint

In addition to the existing conventional smoothness and reference-model constraints that operate on the log-conductivity profile at a given AEM sample, a similarity (or homogeneity) constraint has now been implemented. The similarity constraint penalises an objective function term of the form,

$$\Phi_q = \alpha_q \frac{1}{N_l} \sum_{i=1}^{N_l} (m_i - \bar{m})^2 = \alpha_q \frac{1}{N_l} \boldsymbol{m}^T {\boldsymbol{L}_q}^T \boldsymbol{L}_q \boldsymbol{m} \qquad (2)$$

where m_i is the log-conductivity inversion parameter for the ith layer and $\bar{m}$ is the average log-conductivity over all the N_l model layers. This is implemented with the linear operator matrix, $\mathbf{L}_q$ whose i,jth element is $\left[\mathbf{L}_q\right]_{ij} = 1 - 1/N_l$ for i = j, and $\left[\mathbf{L}_q\right]_{ij} = -1/N_l$ for i ≠ j, where j. The term α_q is a weight that controls the influence of this constraint relative to other constraints in the model regularisation objective function. This constraint has the effect of penalising the difference of any one layer's log-conductivity from the log-mean of all the other layers.

BUNCH BY BUNCH INVERSION

Motivation

We have implemented the concept of a bunch-by-bunch inversion in the program *GALEISBSTDEM* in which several adjacent AEM soundings in the one flight line are inverted jointly. The intention is to provide localised lateral (along-

line) constraint on both the conductivity and system geometry parameters. This is the same motivation as for existing laterally/spatially constrained algorithms (e.g., Brodie and Sambridge, 2006; Viezzoli *et al*. 2008; Brodie and Ley-Cooper, 2018).

We have found that there are two downsides of these existing methods that invert large swathes of data in one inversion problem. The first is that localised noise bursts, isolated to one or a few parts of a flight line(s), can sometime be enough to prevent the whole inversion from converging. This renders the good data useless, or else time-consuming manual culling needs to be applied. The second downside occurs when the data span across significantly different geoelectric domains. In such cases, because there is a single objective function being minimized, data in one domain gets over-fitted at the expense of the other domain being under-fitted. With the bunch-by-bunch approach the idea is to invert a few, perhaps five to ten, adjacent soundings together so that there are enough soundings to provide sufficient along-line lateral constraint on the system geometry paramaters but not so many that we run into the downsides noted above.

Formulation

In the bunch-by-bunch formulation we invert a set number of soundings N_b at once, always from the same flight line. The bunch of soundings to be inverted together are spaced N_a soundings apart (or may be adjacent, $N_a = \mathbf{1}$). Upon completion of the inversion for that bunch, the middle sounding's results are output before moving on to invert the next bunch completely independently. The next bunch may include some of the same soundings as the previous bunch (i.e., overlapping bunches), but is dependent on the selected input dataset sub-sampling rate N_k. Each bunch is inverted on one processor, and bunches are inverted in parallel. The run time is approximately N_b times longer than single sounding inversion.

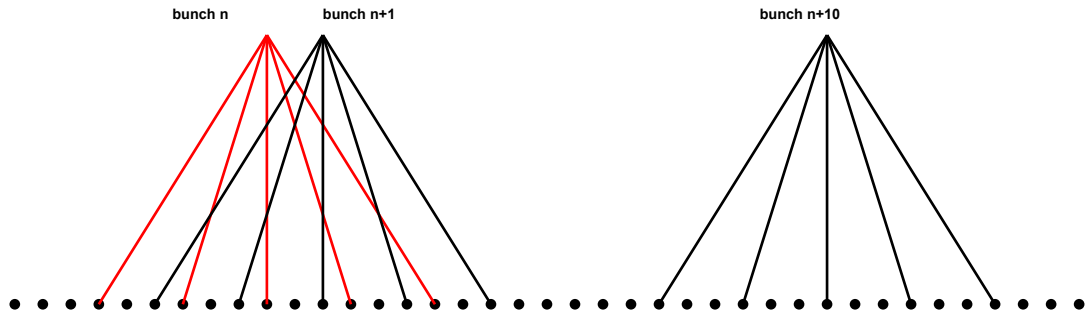

Figure 1. Schematic representation of the bunching method. In this case the number of soundings per bunch is $N_b = 5$ and the bunch adjacency $N_a = 3$, and the input dataset sub-sampling rate is $N_k = 2$. The black dots represent every adjacent sounding in the input dataset.

The input data vector has the same form but is N_b times the size, as in a single-sounding inversion. Likewise, the model parameterisation associates separate 1D layered conductivity profiles and sets of system geometry parameters with each sounding. Unlike the case for holistic inversion (Brodie and Sambridge, 2006), there is no explicit relationship (e.g., splines) between each conductivity profile, or each set of geometry parameters, in the bunch. Instead, several types of lateral (i.e., that operate across the bunch of soundings) constraints may be applied to provide along-line regularisation.

Either first finite difference minimisation (flatness), second finite difference minimisation (smoothness) or similarity type constraints can be applied across the layer log-conductivities of the bunch. For each element of the system geometry parameters the lateral constraints are either second or third finite difference minimisers, or similarity constraints. In this case the second finite difference is equivalent to minimising the absolute accelerations of the receiver-bird relative to the transmitter, which is a physically appealing constraint as this must be the case in reality. For both the conductivity and system geometry parameters, the similarity constraint is analogous to that explained above for vertical conductivity profile in Equation 2. The first, second and third finite difference constraints are implemented via the typical linear operator matrices with rows of the form *[…,-1, 1,…]*, *[…,1, -2, 1,…]*, and *[…,-1, 4, -6, 4, -1,…]* respectively.

We have also trialled a new non-linear constraint that we call a "cable-length" constraint. The motivation behind this is that we know that the length of the receiver bird tow-cable should not vary significantly on a flight, aside from some stretching. Cable-length is a slight misnomer because we actually constrain the straight-line Tx-Rx distance, not the actual slightly curved tow-cable length. This constraint penalises the difference between the modelled Tx-Rx distance for the ith sounding in the bunch, $r_i(\mathbf{m}) = \sqrt{dx_i{}^2 + dy_i{}^2 + dz_i{}^2}$, and some reference value $\hat{r}_i$, via the term,

$$\Phi_l = \alpha_l \frac{1}{N_b} \sum_{i=1}^{N_b} \left(\frac{r_i(\boldsymbol{m}) - \hat{r_l}}{\sigma_l} \right)^2 . \quad (3)$$

Here, σ_l is an uncertainty (i.e., noise or tolerance) on the constraint. We have experimented with making the reference value one of three options. The first option sets, $\hat{r_l} = l_i$, the input observed (measured or assumed) cable-length distance for each sounding, which penalises the difference between the modelled and observed cable-length for each sounding in the bunch. The second option, $\hat{r_l} = 1/N_b \sum_{i=1}^{N_b} l_i$), penalises the difference between modelled and the bunch-average observed cable-length. The third option, $\hat{r_l} = \overline{r(\boldsymbol{m})}$, penalises the difference between the modelled cable-length and the bunch-average modelled cable-length, which is a type of similarity constraint. The non-linear cable-length constraint is akin to a data-misfit objective function term, however where the "data" are not AEM measurements but are one of the versions of $\hat{r_{l_i}}$ given above. As such it cannot be implemented using simple linear operator matrices as in Equation 2. Rather, at each iteration n, it requires calculation of $\mathbf{r}(\mathbf{m_n})$ and its partial derivative matrix (Jacobian), $[\mathbf{J}]_{ij} = \partial r_i(\mathbf{m})/\partial \mathrm{m}_j$, to allow linearisation of $\mathrm{r}(\mathbf{m_{n+1}}) \cong \mathrm{r}(\mathbf{m_n} + \mathbf{J}\Delta\mathbf{m_n})$ about the current model $\mathbf{m_n}$.

Examples

To demonstrate the modifications to the algorithm we will use a 15 km portion of flight line 1007001 from the AusAEM East Yilgarn survey that was acquired with the TEMPEST® AEM system in 2020. We typically find that we cannot adequately fit the data to the ascribed noise levels using Tx-Rx horizontal (Dx) and vertical (Dz) separations measured via the GPS units located on the aircraft and receiver bird, and the receiver pitch (RxP) measured by the receiver bird's inertial measurement unit (IMU). That was also the case for this particular flight line.

Figure 2 shows the results from our joint X- and Z- vector component inversion using the single-sounding inversion algorithm of the previous code where we have inverted for Dx, Dz and RxP. The top three panels show the measured (black line) and inverted (red line) elements of the system geometry. The fourth panel shows the data misfit, PhiD, which would be unity if the data were fit to the ascribed noise level. The bottom panel shows the resulting conductivity-depth section. The inversion has fit the data relatively well on the western side (left) of the section where the conductive cover appears thicker. However, there are numerous vertical striations that detract from the appearance of the section, particularly west of line distance 35,000 m. These correspond with implausible sharp variation or roughness in the inverted system geometry parameters (especially Dz and RxP), which is thought to be caused by instability in the previous algorithm's line-search.

Figure 3 shows the results for the same single-sounding ($N_b = 1$) inversion setup as that in Figure 2, but here we have used the new program. The new code employs a more conservative line-search for both the regularisation parameter at each iteration, and the parameter change step-length within every regularisation parameter line-search trial. This more conservative search, which takes longer but is more robust, has cleaned-up many of the narrow vertical striation and associated roughness in the inverted system geometry parameters.

On the eastern end (right) of the flight line the X- and Z-vector component inversions in Figure 2 and Figure 3 are not fitting the data well. This is likely to be due partly to some features that break up the 1D nature of the geology (e.g. at line distance 42,500 m) and also discrepancies between the true and measured system geometry. Our XZ-amplitude inversion, shown in Figure 4, fits the data significantly better on the eastern end of the flight line and results in a more aesthetic section with fewer obvious artefacts emerging up from the bottom of the section than in Figure 3. It is no surprise that the XZ-amplitude inversion is able to fit the data easier since it has less information content (having lost the vector components) and there is no requirement to either measure or solve for the receiver pitch. We cannot be certain to what extent the apparent "simplification" of the conductivity structure in Figure 4 compared to Figure 3, is due to better data fitting, and to what extent it is due to loss of information content. Our preference would be to fit the vector component data better and maintain all the information.

An example of the results of our bunch-by-bunch inversion is shown in Figure 5. In this example we have inverted five soundings at a time ($\mathrm{N_b} = 5$) spaced three soundings apart ($N_a = 3$) in the new program. This means that there is approximately 150 m between the first and last sounding in the bunch. Lateral smoothness constraints (2nd finite difference) have been applied along-line to the conductivity and also to each of the three system geometry elements that were solved for. Comparison of the new program's X- and Z-vector component single-sounding inversion (Figure 3) with the bunch-by-bunch inversion (Figure 5), shows that there has been an improvement in the data misfits at the eastern end of the line in the bunch-by-bunch inversion. However, we are not claiming that there is an improvement in the overall interpretability of the section.

While the misfits have improved in Figure 5 they were not reduced to an acceptable level of fit (PhiD=1), as they were for much of the line to the east of line distance ~41,500 m in the XZ-amplitude inversion (Figure 4). There has actually been an improvement in the data misfit at line distance ~41,000 m for the bunch-by-bunch inversion compared to the XZ-amplitude inversion, with an associated improvement in the roughness of the Dz system geometry inversion parameter. This is encouraging, however we would still prefer to be able to fit the XZ-vector component data to the

ascribed noise levels everywhere that the geology is quasi-1D. At the time of writing we are still investigating the possible reasons for being unable to fit the data.

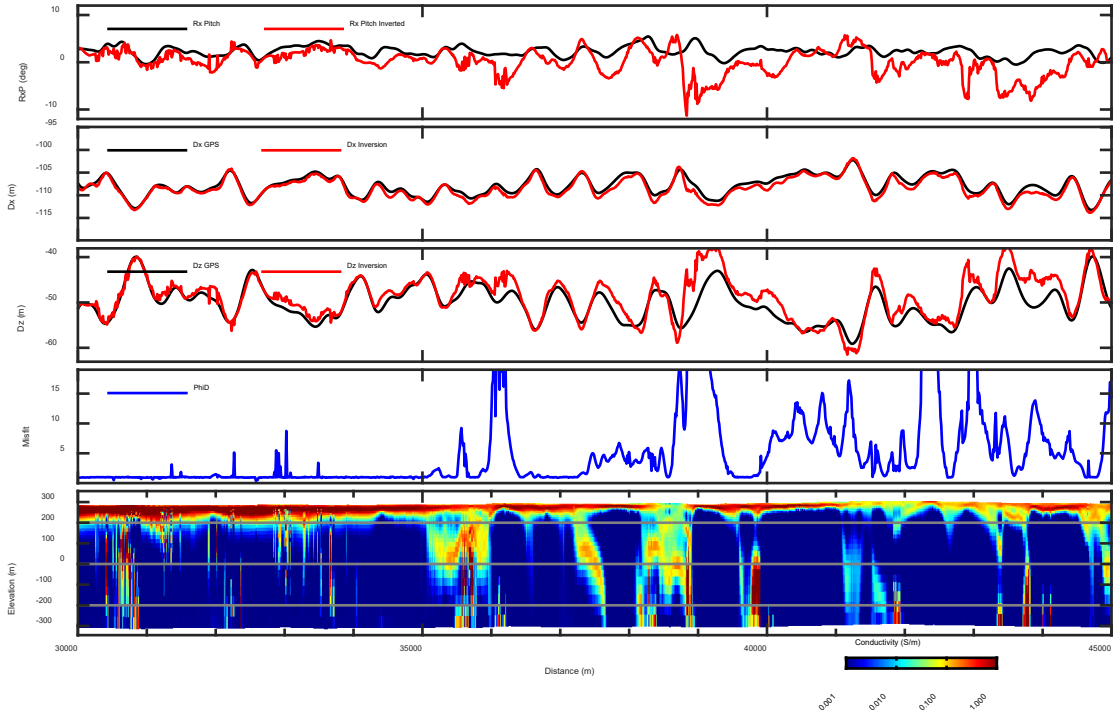

Figure 2. Summary of inversion results for an X and Z vector component joint inversion using the previous program. The top three panels show the measured (black) and inverted (red) system geometry parameters. The bottom two panel show the data misfit and the resulting conductivity section. Numerous narrow vertical striations with corresponding implausible roughness of the inverted system geometry parameters are evident.

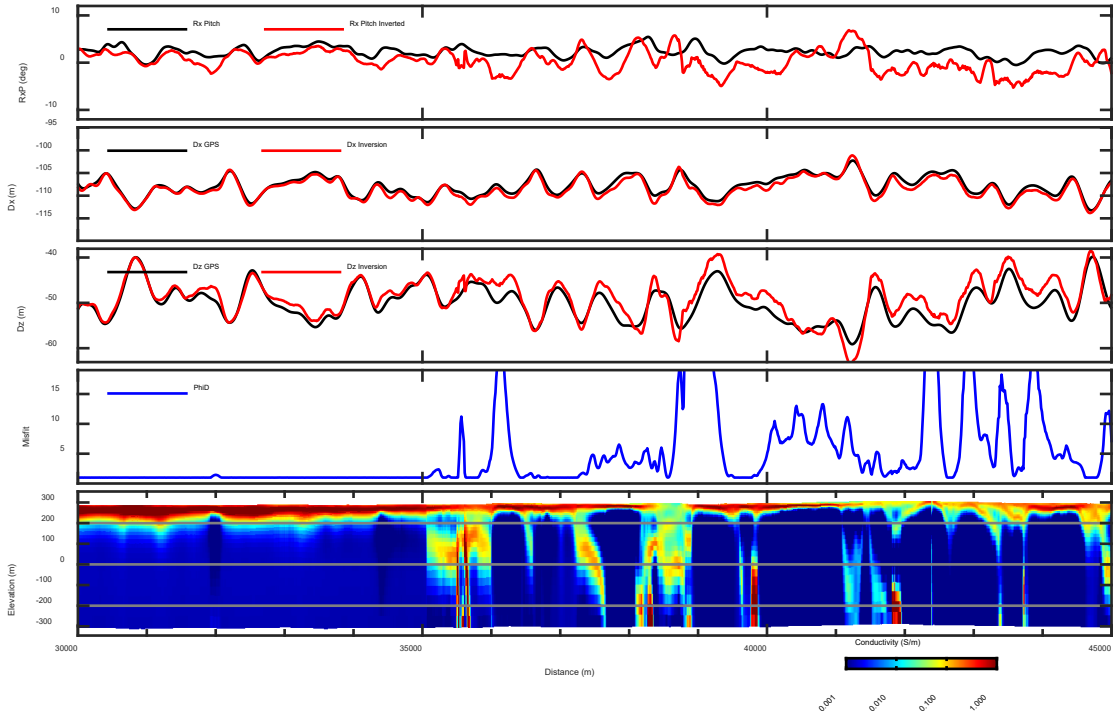

Figure 3. The same summary inversion results as shown in Figure 2, however using the improved inversion program. Comparison to Figure 2 shows that the majority of the narrow vertical striations in the section and associated implausible roughness in the system geometry inversion parameters have been removed.

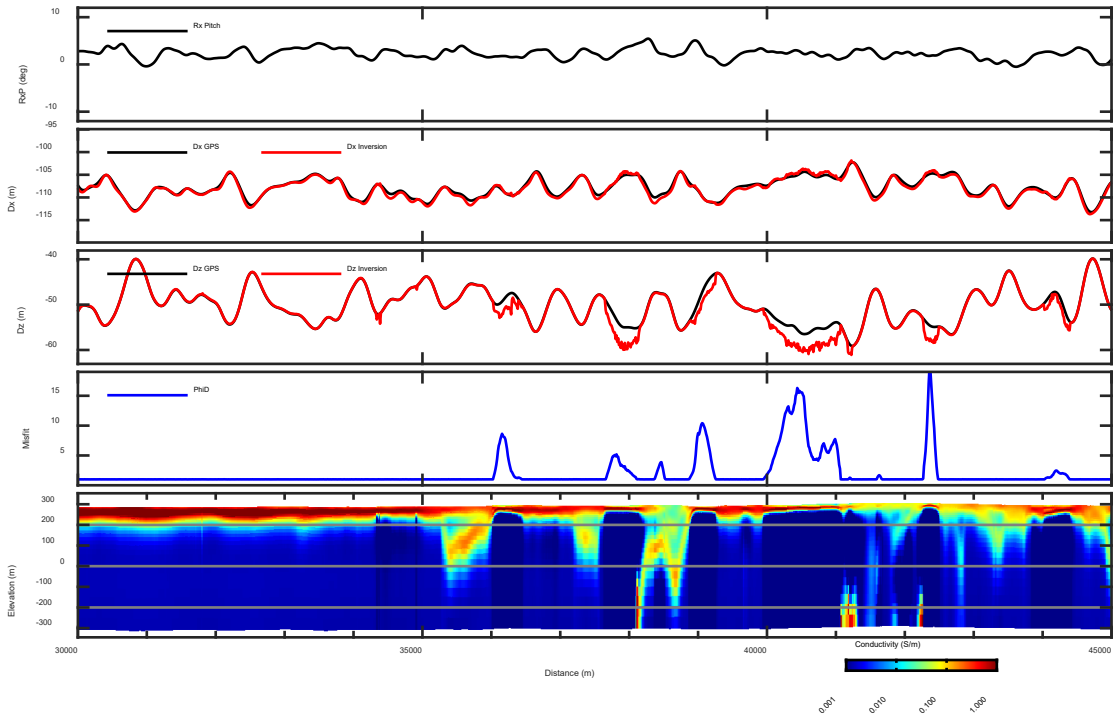

Figure 4. The same summary inversion results as shown in Figure 2 and Figure 3, however inverted using the XZ-amplitude data in the new inversion program. Note that there is not a trace line in the upper panel because the receiver pitch is not solved for in an XZ-amplitude inversion. Comparison to Figure 3 shows that the XZ-amplitude inversion is able to fit the data over a greater proportion of the flight line and results in a more aesthetic section with fewer artefacts.

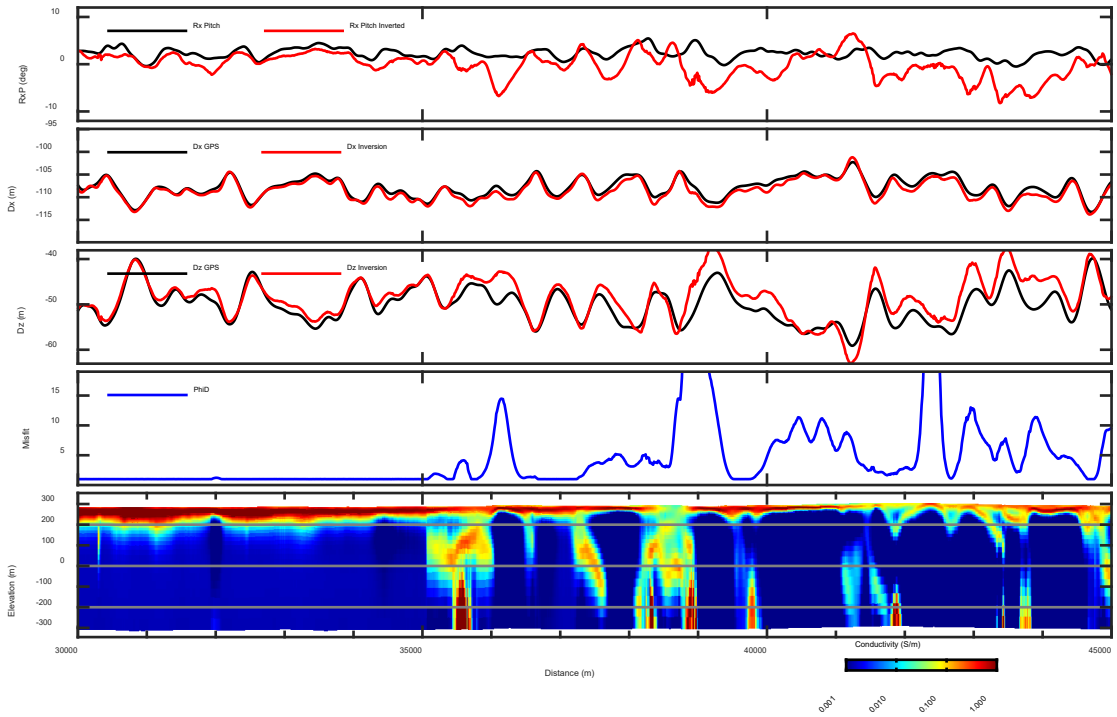

Figure 5. The same summary inversion results as shown in Figure 2 and Figure 3, however this time we have inverted five soundings at a time ($N_b = 5$) spaced three soundings apart ($N_a = 3$) using the bunch by bunch functionality in the new program.

DISCUSSION

Several improvements have been made to the 1D deterministic AEM inversion program *GALEISBSTDEM* that will be publicly released in 2023. They updates range from rudimentary ease of use improvements to the implementation of XZ-amplitude inversion, more conservative line-searches, additional constraint types and the concept of bunch-by-bunch inversion. We have found that the more conservative line-searches have improved the robustness of the inversion resulting in fewer vertical striation artefacts. As previously reported, the XZ-amplitude inversion allows the data to be fitted easier and results in more spatially coherent conductivity sections. The bunch-by-bunch inversion has not so far delivered the improvements in the XZ-vector component inversion that we had hoped for. It has however, improved the data misfits compared to the corresponding single-sounding inversions, and the along-line smoothness of the inverted system geometry parameters. Further work is required to understand why the XZ-vector component inversion formulation does not always fit the data to our satisfaction.

ACKNOWLEDGMENTS

This work was completed as part of a Geoscience Australia-CSIRO placement. The authors would like to acknowledge CSIRO Deep Earth Imaging Future Science Platform (DEI-FSP), CSIRO Discovery Program and CSIRO Research Office for funding and facilitating the placement and Geoscience Australia for supporting the initiative. This abstract is published with the permission of the CEO, Geoscience Australia.

REFERENCES

Brodie, R. and Sambridge, M., 2006. A holistic approach to inversion of frequency-domain airborne EM data. Geophysics 71(6), G301-G312.

Brodie, R.C. and Richardson, M., 2015. Open Source Software for 1D Airborne Electromagnetic Inversion. Extended Abstracts, ASEG-PESA: 24th International Geophysical Conference and Exhibition, Perth, Australia.

Brodie, R.C., 2015, GALEISBSTDEM: A deterministic algorithm for 1D sample by sample inversion of time-domain AEM data – theoretical details. Online: https://github.com/GeoscienceAustralia/ga-aem.git.

Brodie, R.C., and Ley-Cooper, A.Y., 2018, Spatially and conductivity log constrained AEM inversion: Extended Abstracts, 1st AEGC: Innovation and Integration, Sydney, Australia.

Combrinck, M., and Wright, I.R., 2022, AEM base frequency and depth of investigation: Extended Abstracts, 17th SAGA Biennial Conference and Exhibition, Sun City, South Africa.

Constable, S.C., Parker, R.L., and Constable, C.G., 1987, Occam's inversion; a practical algorithm for generating smooth models from electromagnetic sounding data. Geophysics 52, 289-300.

Fitzpatrick A., and Whitford, M., 2019, Strategic electromagnetic geophysical prospecting across a belt - an example over the Albany Fraser Orogen, Extended Abstracts, 2nd AEGC: From Data to Discovery, Perth, Australia. DOI: 10.1080/22020586.2019.12073081.

Ley-Cooper, A.Y., and Richardson, M., 2018, AusAEM; acquisition of AEM at an unprecedented scale: Extended Abstracts, 1st AEGC: Innovation and Integration, Sydney, Australia.

Ley-Cooper, A.Y., Roach, I.C., and Brodie, R.C., 2019, Geological insights of Northern Australia's AusAEM airborne EM survey: Extended Abstracts, 2nd AEGC: From Data to Discovery, Perth, Australia.

Minsley, B.J., Rigby, J.R., James, S.R., Burton, B.L., Knierim, K.J., Pace, M.D., and Kress, W.H., 2021, Airborne geophysical surveys of the lower Mississippi Valley demonstrate system-scale mapping of subsurface architecture. Communications Earth & Environment, 2(1), 1-14.

Viezzoli, A., Christiansen, A. V., Auken, E. and Sorensen, K., 2008. Quasi-3D modeling of airborne TEM data by spatially constrained inversion. Geophysics 73(3), F105-F113.